ÖAW Austrian Academy of Sciences

Doctoral Program
Computational Mathematics
Numerical Analysis and Symbolic Computation

JKU JOHANNES KEPLER UNIVERSITY LINZ

Adaptive space-time finite element methods for parabolic optimal control problems

Ulrich Langer Andreas Schafelner

DK-Report No. 2021-07 05 2021

A–4040 LINZ, ALTENBERGERSTRASSE 69, AUSTRIA

Supported by

Austrian Science Fund (FWF) Upper Austria

FWF Der Wissenschaftsfonds.

LAND OBERÖSTERREICH

DK sponsors:

- **Johannes Kepler University Linz** (JKU)
- **Austrian Science Fund** (FWF)
- **Upper Austria**

Adaptive space-time finite element methods for parabolic optimal control problems*

Ulrich Langer[1] and Andreas Schafelner[2]

[1] *Institute for Computational Mathematics*
Johannes Kepler University Linz
Altenbergerstr. 69, 4040 Linz, Austria
[2] *Doctoral Program "Computational Mathematics"*
Johannes Kepler University Linz
Altenbergerstr. 69, A-4040 Linz, Austria

Abstract

We present, analyze and test locally stabilized space-time finite element methods on fully unstructured simplicial space-time meshes for the numerical solution of space-time tracking parabolic optimal control problems with the standard L_2-regularization. We derive a priori discretization error estimates in terms of the local mesh-sizes for shape-regular meshes. The adaptive version is driven by local residual error indicators. We perform numerical tests for benchmark examples having different features. In particular, we consider a discontinuous target in form of a first expanding and then contracting ball in 3d that is fixed in the 4d space-time cylinder.

Keywords: parabolic optimal control problem, L_2-regularization, space-time finite element methods, discretization error estimates, adaptive versions, parallel solvers

2010 MSC: 49J20, 35K20, 65M60, 65M50, 65M15, 65Y05

1 Introduction

Let us consider the following space-time tracking optimal control problem: For a given target function $y_d \in L_2(Q)$ (desired state) and for some appropriately chosen regularization (cost) parameter $\varrho > 0$, find the state $y \in Y$ and the control $u \in U$ minimizing the cost functional

$$J(y,u) = \frac{1}{2}\int_Q |y - y_d|^2 \, \mathrm{d}Q + \frac{\varrho}{2}\|u\|_U^2 \tag{1}$$

subject to the linear parabolic initial-boundary value problem (IBVP)

$$\partial_t y - \mathrm{div}_x(\nu \nabla_x y) = u \text{ in } Q, \quad y = 0 \text{ on } \Sigma, \quad y = 0 \text{ on } \Sigma_0, \tag{2}$$

*The authors would like to thank the Austrian Science Fund (FWF) for the financial support under the grant DK W1214-04.

where $Q := \Omega \times (0,T)$, $\Sigma := \partial\Omega \times (0,T)$, $\Sigma_0 := \Omega \times \{0\}$, $T > 0$ is the final time, ∂_t denotes the partial time derivative, div_x is the spatial divergence operator, ∇_x is the spatial gradient, and the source term u on the right-hand side of the parabolic PDE (2) serves as control. The spatial domain $\Omega \subset \mathbb{R}^d$, $d = 1, 2, 3$, is supposed to be bounded and Lipschitz. The coefficient ν is assumed to be uniformly positive and bounded, i.e., there exist positive constants ν_1 and ν_2 such that

$$0 < \nu_1 \le \nu(x,t) \le \nu_2 \quad \text{for almost all } (x,t) \in Q. \tag{3}$$

For simplicity, we here consider only scalar coefficients, but it is clear that the scalar coefficient ν can be replaced by a symmetric, and uniformly positive definite and bounded $d \times d$ coefficient matrix.

In the standard setting, that was already investigated in the famous book by J.L. Lions [34], the distributed control u is taken from $U = L_2(0,T;L_2(\Omega)) = L_2(Q)$, and thus the cost of the control is also measured in the $L_2(Q)$-norm that mathematically serves as regularization term in (1). Since the state equation (2) has a unique solution $y \in Y := Y_0 = \{v \in L^2(0,T;H^1_0(\Omega)) : \partial_t v \in L^2(0,T;H^{-1}(\Omega)),\ v = 0 \text{ on } \Sigma_0\} = \{v \in W(0,T) : v = 0 \text{ on } \Sigma_0\}$, one can conclude the existence of a unique control $u \in U$ minimizing the cost functional $J(Su,u)$, where S is the solution operator mapping $u \in U$ to the unique solution $y \in Y$ of (2); see, e.g., [34] and [50]. There is a huge number of publications devoted to the numerical solution of optimal control problems (1)–(2) with the standard L_2-regularization; see, e.g., [22, 50, 6]. The overwhelming majority of the publications uses some time-stepping method or discontinuous Galerkin method for the time discretization in combination with some space-discretization method like the finite element method; see, e.g., [36, 37]. The unique solvability of the optimal control problem can also be established by showing that the optimality system (KKT system) has a unique solution, since these problems are equivalent for quadratic cost functionals with linear constraints. In [33], the Banach-Nečas-Babuška (BNB) theorem was applied to the optimality system to show its well-posedness. We refer the reader to [7, Theorem 3.6] and [15, Theorem 2.6] for the version of the BNB theorem, which was used in [33], and to the original papers [40, 3]. Furthermore, the discrete inf-sup condition, that does not follow from the inf-sup condition in the infinite-dimensional setting, was established for continuous space-time finite element discretizations on fully unstructured simplicial space-time meshes. The discrete inf-sup condition implies stability of the discretization and a priori discretization error estimates; see also [3, 4]. In connection with continuous space-time finite element discretizations for parabolic optimal control problems, we would like to mention the publications [18] and [39]. A comprehensive overview of space-time methods for parabolic IBVP can be found in [48].

Beside the L_2-regularization, other regularization respectively cost terms can be chosen in order to obtain certain desired effects. We here only mention the sparsity techniques where the L_1 term $\mu\|u\|_{L_1(Q)}$ with the sparsity parameter μ is added to the L_2-regularization term and directional sparsity techniques [45, 20, 11], control in measure spaces also leading to locally concentrated controls [10], and the energy regularization where $U = L^2(0,T;H^{-1}(\Omega))$ [32]. The energy regularization is motivated by applications in electrical engineering where controls u from $L^2(0,T;H^{-1}(\Omega))$ are admissible, i.e. controls that are concentrated on spatial hypersurfaces. Furthermore, the observation can be restricted

to some subset of the space-time cylinder $\overline{Q}$ including $\Sigma_T := \Omega \times \{0\}$ (observation at the terminal time), or the control can be restricted to some subset of $\overline{Q}$ including the boundary Σ or some parts of Σ (control via Dirichlet, Neumann, and Robin boundary conditions).

In this paper, we consider locally stabilized space-time finite element methods on fully unstructured simplicial space-time meshes for the numerical solution of the space-time tracking parabolic optimal control problem (1)–(2) with the standard L_2-regularization as model problem, although the space-time finite element technique presented in this paper can certainly be applied to other optimal control problems as well. In our former works [29, 30, 30], we have successfully applied the locally stabilized space-time finite element methods to the state equation (2) with right-hand sides u from $L_2(Q)$ and with special distributional right-hand sides u from $L^2(0,T;H^{-1}(\Omega))$. In particular, we have proposed adaptive space-time finite element schemes based on local error indicators that are derived from the residual error indicator proposed in [47], and Repin's functional error estimator providing a guaranteed upper bound for any admissible approximation [42]. In our note [31], we report on the first results for globally stabilized space-time finite element methods applied to the optimal control problem (1)–(2), but on quasi-uniform meshes characterized by a global mesh-size parameter h. Here we use global time-upwind finite element test functions $v_h + \theta h^2 \partial_t v_h$ and $q_h - \theta h^2 \partial_t q_h$ for constructing consistent finite element schemes approximating the reduced optimality system. We mention that upwind test functions were introduced by Hughes and Brooks for constructing stable finite element schemes for stationary convection-diffusion problems in [23]. This stabilization technique is called SUPG, and was later used by Johnson and Saranen [25] for transient problems; see also [24] for the related Galerkin Least-Squares finite element methods, and [28, 5] for more recent papers on these stabilization techniques. In the case of unstructured, but shape-regular meshes naturally produced by adaptive schemes, one should replace the global discretization parameter h by the local mesh-size h_K that can be different for every element K from the triangulation $\mathcal{T}_h$. This simple replacement of h by h_K works well for the state equation alone [29, 30, 30], but not for the reduced optimality system. Therefore, in this paper, we introduce a differentiable mesh-density function $\lambda_h(x,t)$ in order to prove coercivity of the mesh-dependent bilinear form $a_h(\cdot,\cdot)$ that corresponds to the finite element scheme for the reduced optimality system. Coercivity together with Galerkin orthogonality and extended boundedness immediately leads to a best-approximation estimate from which one can derive convergence rate estimates by means of interpolation error estimates under additional regularity assumptions. Now adaptivity can be performed simultaneously in space and time on the basis of local error indicators. We use the residual error indicator that was introduced for the state equation in [47]. Finally, we have to solve one system of finite element equation for defining all space-time unknowns all at once. The system matrix is non-symmetric, but positive definite. We solve this system by means of a parallel version of the flexible General Minimal Residual (FGMRES) method [43], preconditioned by a block-diagonal algebraic multigrid (AMG) preconditioner. The parallelization is relatively easy since it can be done simultaneously in space and time as known from elliptic problems.

The remainder of the paper is organized as follows. Section 2 introduces the basic notations and states some preliminary results on the solvability and

the space-time discretization of the parabolic initial-boundary value problem (2) that serves as state equation in the optimal control problem studied in this paper. Section 3 states the reduced optimality system characterizing the unique solution of the optimal control problem (1)–(2). The space-time finite element discretization of the reduced optimality system is derived in Section 4. In Section 5, we establish the coercivity of the bilinear form corresponding the finite element scheme. A priori estimates of the discretization error are derived in Section 6. Section 7 briefly describes the construction of simultaneous space-time adaptive finite element schemes. The algebraic system corresponding to the finite element scheme and the solver are presented in Section 8. Section 9 is devoted to the presentation and discussion of the numerical results. Finally, we draw some conclusion and give an outlook in Section 10.

2 Preliminaries

Throughout the paper, we use the standard notations for Lebesgue spaces $L_p(\cdot)$ and Sobolev spaces $W_p^k(\cdot)$ respectively (resp.) $H^k(\cdot) = W_2^k(\cdot)$ with the corresponding norms resp. scalar products; see, e.g., [1]. Furthermore, we also use Bochner spaces $L_2(0,T;X)$ of square-integrable abstract functions, mapping the time interval $(0,T)$ to the spatial Hilbert space $X = L_2(\Omega), H_0^1(\Omega), H^{-1}(\Omega), \ldots$; see, e.g., [34] for the precise definition of the spaces, norms and scalar products as well as for the main properties.

The standard weak or variational formulation of the state equation (2) reads as follows: Find $y \in Y = Y_0 := \{y \in V : \partial_t y \in V^*,\ v = 0 \text{ on } \Sigma_0\}$ such that

$$b(y,v) = \langle u, v\rangle_Q \quad \forall v \in V := L_2(0,T;H_0^1(\Omega)) \tag{4}$$

with the bilinear form $b(\cdot,\cdot) : Y \times V \longrightarrow \mathbb{R}$, defined by the identity

$$b(y,v) := \int_Q \Big[\partial_t y\, v + \nu \nabla_x y \cdot \nabla_x v\Big]\, \mathrm{d}Q, \quad \forall (y,v) \in Y \times V, \tag{5}$$

and the duality product $\langle\cdot,\cdot\rangle_Q : V^* \times V \longrightarrow \mathbb{R}$, and for given $u \in V^*$. We mention that the first integral in (5) has to be understood as duality pairing as well since $\partial_t y$, in general, belongs to V^*. We also may integrate by parts with respect to time. Then we can include the initial conditions as natural conditions into the variational formulation, and we look for a weak solution y in $H_0^{1,0}(Q)$ with test function v from $H_0^{1,1}(Q)$ vanishing on the top $\Sigma_T := \Omega \times \{T\}$ of the space-time cylinder Q; see, e.g., [26]. The standard methods to show existence and uniqueness are Galerkin's method in space and a priori estimates. One can also use the BNB theorem as it was done in [46]. Indeed, the bilinear form $b(\cdot,\cdot)$ fulfills the following three conditions:

(BNB1) boundedness: $|b(y,v)| \le c_{\mathrm{b}} \|y\|_Y \|v\|_V$,
(BNB2) inf-sup condition: $\inf_{y\in Y\setminus\{0\}} \sup_{v\in V\setminus\{0\}} \frac{b(y,v)}{\|u\|_U\, \|v\|_V} \ge c_{\mathrm{infsup}} > 0$,
(BNB3) injectivity of B^*: $\forall v \in V \setminus \{0\}\ \exists y \in Y : b(y,v) \neq 0$,

that are sufficient and necessary for $B : Y \to V^*$ being an isomorphism, where the operator B is defined by the bilinear form:

$$\langle By, v\rangle_Q = b(y,v)\ \forall (y,v) \in Y \times V.$$

Therefore, the solution operator $S = B^{-1}$ is a well-defined bounded linear operator from V^* onto Y. Moreover, if $u \in L_2(Q)$, then the unique solution y belongs to the space

$$H^{L,1}(Q) = \{v \in H^1(Q) : L_x v := -\mathrm{div}_x(\nu \nabla_x v) \in L_2(Q)\}$$

provided that the coefficient ν fulfills some additional conditions; see [13]. This property is called maximal parabolic regularity. We mentioned that already Ladyzhenskaya proved maximal parabolic regularity for the case $\nu = 1$ in [26]. Until now many papers have been published on this topic; see, e.g., [17].

3 Optimality System

Eliminating the control u from the optimality system by means of the so-called gradient equation $p + \varrho u = 0$, we get the reduced optimality system the weak form of which reads as follows: Find the state $y \in Y_0$ and the adjoint state $p \in P_T$ such that

$$\varrho \int_Q \Big[\partial_t y\, v + \nu \nabla_x y \cdot \nabla_x v\Big] \mathrm{d}Q + \int_Q p\, v \,\mathrm{d}Q = 0, \tag{6}$$

$$-\int_Q y\, q \,\mathrm{d}Q + \int_Q \Big[-\partial_t p\, q + \nu \nabla_x p \cdot \nabla_x q\Big] \mathrm{d}Q = -\int_Q y_d\, q \,\mathrm{d}Q \tag{7}$$

holds for $v, q \in V$, where $P_T := \{p \in W(0,T) : p = 0 \text{ on } \Sigma_T\}$. It is shown in [33, Theorem 3.3] by means of the BNB theorem that the variational reduced optimality system (6)–(7) is well-posed.

In addition to (3), we assume that the coefficient function $\nu(x,t)$ is of bounded variation in t for almost all $x \in \Omega$. Then we can conclude maximal parabolic regularity for the parabolic equations (6) and (7) because the corresponding right-hand sides $-\frac{1}{\varrho}p$ and $y - y_d$ belong to $L_2(Q)$; see [13]. Therefore, $\partial_t y$ and $L_x y := -\mathrm{div}_x(\nu\, \nabla_x y)$ as well as $\partial_t p$ and $L_x p$ belong to $L_2(Q)$ too. In this case, the variational reduced optimality system (6)–(7) can be rewritten in the strong form as coupled forward and backward system of parabolic PDEs: Find $y \in Y_0 \cap H^{L,1}(Q)$ and $p \in P_T \cap H^{L,1}(Q)$ such that the coupled PDE optimality system

$$\varrho\Big[\partial_t y - \mathrm{div}_x(\nu \nabla_x y)\Big] = -p \quad \text{in } L_2(Q), \tag{8}$$

$$-\partial_t p - \mathrm{div}_x(\nu\, \nabla_x p) = y - y_d \quad \text{in } L_2(Q) \tag{9}$$

holds. Further regularity results for parabolic problems can be found, e.g., in [27] and [16]. Later we need such regularity results for convergence rate estimates.

4 Space-time finite element discretization

We now use the PDE optimality system (8)–(9) as starting point for constructing stable and consistent space-time finite element schemes on fully unstructured simplicial triangulations of the space-time cylinder Q.

Thus, let us first consider a decomposition $\mathcal{T}_h = \{K\}$ of Q into shape-regular simplicial elements, i.e., $\overline{Q} = \bigcup_{K \in \mathcal{T}_h} \overline{K}$, and $K \cap K' = \emptyset$ for all K and K' from

$\mathcal{T}_h$ with $K \neq K'$; see, e.g., [7, 15] for more details. Once a shape-regular triangulations is available, we define the space-time finite element spaces $Y_{0h} = \{y_h \in S_h^k(\overline{Q}) : y_h = 0 \text{ on } \overline{\Sigma} \cap \overline{\Sigma}_0\}$ and $P_{Th} = \{p_h \in S_h^k(\overline{Q}) : p_h = 0 \text{ on } \overline{\Sigma} \cap \overline{\Sigma}_T\}$. The standard finite element space

$$S_h^k(\overline{Q}) = \{y_h \in C(\overline{Q}) : y_h(x_K(\cdot)) \in \mathbb{P}_k(\hat{K}),\, \forall K \in \mathcal{T}_h\}$$

consists of all continuous and piecewise polynomial functions (provided that $x_K(\cdot)$ is affine-linear), where $x_K(\cdot)$ denotes the map from the reference element $\hat{K}$ (unit simplex) to the finite element $K \in \mathcal{T}_h$, and $\mathbb{P}_k(\hat{K})$ is the space of polynomials of the degree $k \in \mathbb{N} := \{1, 2, \ldots\}$ on the reference element $\hat{K}$.

In addition to the assumptions made above, we further assume that ν is piecewise smooth in the sense that $\mathrm{div}_x(\nu \nabla_x w_h)|_K \in L_2(K)$ for all w_h from Y_{0h} or P_{Th} and for all $K \in \mathcal{T}_h$. Now we multiply the first PDE (8) by a upwind test function $v_h + \theta\lambda_h^2 \partial_t v_h$ with $v_h \in Y_{0h}$, and the second one (9) by $q_h - \theta\lambda_h^2 \partial_t q_h$ with $q_h \in P_{Th}$, where θ is some positive scaling parameter and $\lambda_h \in W_\infty^1(Q)$ is a mesh-density function which we will choose later. Then, integrating over K, integrating by parts in the elliptic terms where the scaling parameter θ does not appear, and summing over all $K \in \mathcal{T}_h$, we arrive at the variational consistency identity

$$a_h(y, p; v_h, q_h) = \ell_h(v_h, q_h) \quad \forall (v_h, q_h) \in Y_{0h} \times P_{Th}, \tag{10}$$

with the combined bilinear and linear forms

$$\begin{aligned} a_h(y, p; v, q) \;=\; & \sum_{K \in \mathcal{T}_h} \int_K \Big[\varrho\big(\partial_t y\, v + \theta\lambda_h^2 \partial_t y \partial_t v + \nu \nabla_x y \cdot \nabla_x v + \theta\lambda_h^2 L_x y\, \partial_t v\big) \\ & + p(v + \theta\lambda_h^2 \partial_t v) - \partial_t p\, q + \theta\lambda_h^2 \partial_t p \partial_t q + \nu \nabla_x p \cdot \nabla_x q \\ & - \theta\lambda_h^2 L_x p\, \partial_t q - y(q - \theta\lambda_h^2 \partial_t q) \Big]\, \mathrm{d}K, \quad \text{and} \end{aligned} \tag{11}$$

$$\ell_h(v, q) \;=\; -\sum_{K \in \mathcal{T}_h} \int_K y_d(q - \theta\lambda_h^2 \partial_t q)\, \mathrm{d}K, \tag{12}$$

respectively. The continuous and piecewise differentiable mesh-density function $\lambda_h(x, t)$ should be chosen in such a way that the inequalities

$$0 < \underline{\lambda}_0 h_K \leq \lambda_h(x, t) \leq \overline{\lambda}_0 h_K \quad \text{and} \quad |\partial_t \lambda_h(x, t)| \leq \lambda_1 \tag{13}$$

hold for all $(x, t) \in K$, $K \in \mathcal{T}_h$, and for all meshes under consideration, where $h_K = \mathrm{diam}(K)$, and $\underline{\lambda}_0$, $\overline{\lambda}_0$ and λ_1 are some positive generic constants. We can easily define the mesh density function $\lambda_h(x, t)$ by means of the finite element space $S_h^1(\overline{Q}) = \mathrm{span}\{\varphi_i : i = 1, 2, \ldots, n_h\}$, spanned by the nodal basis functions $\varphi_i(x, t)$, as follows

$$\lambda_h(x, t) = \sum_{i=1}^{n_h} h_i \varphi_i(x, t),$$

where h_i denotes the average of the length of all edges meeting at the vertex (x^i, t^i), i.e. the sum of the lengths divided by the number of these edges. We note that $\lambda_h((x^i, t^i)) = h_i$ since $\varphi_j((x^i, t^i)) = \delta_{i,j}$, where $\delta_{i,j}$ denotes Kronecker's symbol. The conformity and the shape regularity of the mesh immediately imply inequalities (13). The general discretization parameter h can be chosen as $(n_h)^{-1/(d+1)}$ or $(N_h)^{-1/(d+1)}$ or $(M_h)^{-1/(d+1)}$, where n_h is the number of

vertices in $\mathcal{T}_h$, $N_h = \dim Y_{0h}$ and $M_h = \dim P_{Th}$. We note that $h_K = O(h)$ for all $K \in \mathcal{T}_h$ in the case of a (quasi) uniform mesh.

The consistent finite element scheme corresponding to (10) now reads as follows: Find $(y_h, p_h) \in Y_{0h} \times P_{Th}$ such that

$$a_h(y_h, p_h; v_h, q_h) = \ell_h(v_h, q_h) \quad \forall (v_h, q_h) \in Y_{0h} \times P_{Th}. \tag{14}$$

Subtracting (14) from (10), we immediately obtain the Galerkin orthogonality relation

$$a_h(y - y_h, p - p_h; v_h, q_h) = 0 \quad \forall\, (v_h, q_h) \in Y_{0h} \times P_{Th}, \tag{15}$$

which is crucial for deriving discretization error estimates.

5 Coercivity and unique solvability

We will now show that the bilinear a_h is coercive on $Y_{0h} \times P_{Th}$ with respect to the norm

$$\|(v, q)\|_h^2 = \|v\|_{h,T}^2 + \|q\|_{h,0}^2, \tag{16}$$

for some suitably chosen scaling parameter θ, with

$$\begin{aligned} \|v\|_{h,T}^2 &= \alpha\varrho\|v(\cdot,T)\|_{L_2(\Omega)}^2 + \varrho\theta\,\|\lambda_h\partial_t v\|_{L_2(Q)}^2 + \varrho\|\sqrt{\nu}\nabla_x v\|_{L_2(Q)}^2 \ \text{ and} \\ \|q\|_{h,0}^2 &= \alpha\|q(\cdot,0)\|_{L_2(\Omega)}^2 + \theta\,\|\lambda_h\partial_t q\|_{L_2(Q)}^2 + \|\sqrt{\nu}\nabla_x q\|_{L_2(Q)}^2, \end{aligned}$$

where α is some positive parameter. We choose $\alpha = 1$ if not stated otherwise. First, we observe that the identity

$$\begin{aligned} a_h(v_h, q_h; v_h, q_h) &= \sum_{K\in\mathcal{T}_h} \int_K \Big[\varrho\big(\partial_t v_h\, v_h + \theta\lambda_h^2|\partial_t v_h|^2 + |\sqrt{\nu}\nabla_x v_h|^2 \\ &\quad + \theta\lambda_h^2 L_x v_h\,\partial_t v_h\big) + q_h(v_h + \theta\lambda_h^2\partial_t v_h) - \partial_t q_h\, q_h + \theta\lambda_h^2|\partial_t q_h|^2 \\ &\quad + |\sqrt{\nu}\nabla_x q_h|^2 - \theta\lambda_h^2 L_x q_h\,\partial_t q_h - v_h(q_h - \theta\lambda_h^2\partial_t q_h)\Big]\,\mathrm{d}K \\ &= \sum_{K\in\mathcal{T}_h} \int_K \varrho\big(\theta\lambda_h^2|\partial_t v_h|^2 + |\sqrt{\nu}\nabla_x v_h|^2 + \theta\lambda_h^2 L_x v_h\,\partial_t v_h\big)\,\mathrm{d}K \\ &\quad + \sum_{K\in\mathcal{T}_h} \int_K \big(\theta\lambda_h^2|\partial_t q_h|^2 + |\sqrt{\nu}\nabla_x q_h|^2 - \theta\lambda_h^2 L_x q_h\,\partial_t q_h\big)\,\mathrm{d}K \\ &\quad + \frac{\varrho}{2}\|v_h(\cdot,T)\|_{L_2(\Omega)}^2 + \frac{1}{2}\|q_h(\cdot,0)\|_{L_2(\Omega)}^2 - \int_Q 2\theta\lambda_h\partial_t\lambda_h v_h q_h \mathrm{d}Q \end{aligned} \tag{17}$$

is valid for all $(v_h, q_h) \in Y_{0h} \times P_{Th}$. Here we have used the identities

$$\int_Q \varrho\partial_t v_h\, v_h \mathrm{d}Q = \frac{\varrho}{2}\|v_h(\cdot,T)\|_{L_2(\Omega)}^2, \quad -\int_Q \partial_t q_h\, q_h \mathrm{d}Q = \frac{1}{2}\|q_h(\cdot,0)\|_{L_2(\Omega)}^2,$$

and

$$\begin{aligned} \int_Q \theta\lambda_h^2 v_h\partial_t q_h &= -\int_Q \theta\partial_t(\lambda_h^2 v_h) q_h \mathrm{d}Q + \int_{\partial Q} \theta\lambda_h^2 v_h q_h \mathrm{d}s \\ &= -\int_Q \theta\lambda_h^2\partial_t v_h q_h \mathrm{d}Q - \int_Q 2\theta\lambda_h\partial_t\lambda_h v_h q_h \mathrm{d}Q. \end{aligned}$$

We note that, in the latter identity, the boundary integral vanishes for all finite element functions (v_h, q_h) from $Y_{0h} \times P_{Th}$.

The special case that

1. $k = 1$ and $\nu = const$ on K for all $K \in \mathcal{T}_h$, and
2. $\partial_t \lambda_h = 0$, e.g. uniform mesh $h_i = h$, as considered in [31],

makes the terms with the second-order elliptic operator L_x and the last term in (17) zero. Then the identity (17) gives

$$a_h(v_h, q_h; v_h, q_h) = \mu_c \|(v, q)\|_h^2 \quad \forall (v_h, q_h) \in Y_{0h} \times P_{Th}$$

with $\mu_c = 1$ provided that α is chosen as 0.5 in the definition of the norm (16), i.e., the bilinear form is coercive on $Y_{0h} \times P_{Th}$ with the coercivity constant 1.

In the general case, we have to estimate these terms. Beside Cauchy's and Young's inequalities, we need the generalized Friedrichs' inequality

$$\|v\|_{L_2(Q)} \le c_{\mathrm{F}}(\nu) \|\sqrt{\nu} \nabla_x v\|_{L_2(Q)} \; \forall v \in V = L_2(0, T; H_0^1(\Omega)), \tag{18}$$

where $c_F(\nu)$ can obviously be estimated from above by the Friedrichs constant $c_{\mathrm{F},\Omega}$ of the spatial domain Ω times $(\nu_1)^{-1/2}$, i.e. $c_{\mathrm{F}}(\nu) \le c_{\mathrm{F},\Omega}/\nu_1^{1/2}$, and the special inverse inequality

$$\lambda_{\max,K} := \max_{\mathbf{w}_h \in \nabla_x S_h^k(\overline{K})} \frac{(\mathrm{div}_x(\nu \mathbf{w}_h), \mathrm{div}_x(\nu \mathbf{w}_h))_{L_2(K)}}{(\sqrt{\nu}\mathbf{w}_h, \sqrt{\nu}\mathbf{w}_h)_{L_2(K)}} \le c_{\mathrm{inv},K}^2 h_K^{-2}, \tag{19}$$

where $\lambda_{\max,K}$ can be computed from a small generalized matrix eigenvalue problem for every finite element $K \in \mathcal{T}_h$ [29]. The upper bound can be shown by mapping K to the reference element $\hat{K}$. Now, using these inequalities, we can proceed to estimate (17) from below as follows:

$$\begin{aligned}
&a_h(v_h, q_h; v_h, q_h) \ge \frac{\varrho}{2} \|v_h(\cdot, T)\|_{L_2(\Omega)}^2 + \frac{1}{2} \|q_h(\cdot, 0)\|_{L_2(\Omega)}^2 \\
&+ \sum_{K \in \mathcal{T}_h} \int_K \varrho \big[\theta \lambda_h^2 (1 - \frac{1}{2\varepsilon}) |\partial_t v_h|^2 + (1 - \varepsilon \theta a_K - \theta b \varrho^{-1}) |\sqrt{\nu} \nabla_x v_h|^2\big] \, \mathrm{d}K \\
&+ \sum_{K \in \mathcal{T}_h} \int_K \big[\theta \lambda_h^2 (1 - \frac{1}{2\epsilon}) |\partial_t v_h|^2 + (1 - \epsilon \theta a_K - \theta b) |\sqrt{\nu} \nabla_x v_h|^2\big] \, \mathrm{d}K \\
&\ge \mu_c \, \|(v_h, q_h)\|_h^2 \quad \forall \, (v_h, q_h) \in Y_{0h} \times P_{Th},
\end{aligned} \tag{20}$$

where ε and ϵ are positive parameters from Young's inequalities, $c_{\mathrm{F}} = c_{\mathrm{F}}(\nu)$, $a_K = 0.5 \overline{\lambda}_0^2 c_{\mathrm{inv},K}^2$, $b = \overline{\lambda}_0 \lambda_1 h c_{\mathrm{F}}^2$, and $h = \max_{K \in \mathcal{T}_h} h_K$. The coercivity constant μ_c is positive for properly chosen positive parameters ε, ϵ, and θ. Indeed, $\mu_c = 1/2$, if $\varepsilon = 1$, $\epsilon = 1$, and

$$0 < \theta \le \frac{1}{2} \min \Big\{ \frac{\varrho}{\varrho a + b}, \frac{1}{a + b} \Big\}, \tag{21}$$

with $a = \max_{K \in \mathcal{T}_h} a_K$.

The coercivity (20) of the bilinear form a_h on $Y_{0h} \times P_{Th}$ immediately implies that the finite element scheme (14) can only have one solution, but, in the finite dimensional case, uniqueness yields existence. Thus, the space-time finite element scheme (14) has a unique solution that can be determined via the solution of corresponding algebraic system of finite element equations; see Section 8.

Remark. *In the case of a quasi-uniform mesh, formally defined by the setting* $h_K = h$ *and* $h_i = h$, *i.e.* $\lambda_h = h$, $\partial_t \lambda_h = 0$, *and, therefore,* $\underline{\lambda}_0 = \overline{\lambda}_0 = 1$ *and* $\lambda_1 = 0$, *the coercivity estimate* (20) *yields the coercivity estimate presented in [31]. We note that, for* $k = 1$, $L_x v_h = L_x q_h = 0$ *on* $K \in \mathcal{T}_h$ *for all* $(v_h, q_h) \in Y_{0h} \times P_{Th}$ *provided that* ν *is elementwise constant.*

6 A priori discretization error estimates

In order to derive a priori discretization error estimates, we first need to establish the extended boundedness of the bilinear form

$$|a_h(y,p;v_h,q_h)| \le \mu_b \|(y,p)\|_{h,*} \|(v_h,q_h)\|_h \quad \forall (v_h,q_h) \in Y_{0h} \times P_{Th}, \tag{22}$$

and for all $y \in Y_{0h} + Y_0 \cap H^{L,1}(Q)$ and $p \in P_{Th} + P_T \cap H^{L,1}(Q)$, where

$$\begin{aligned} \|(y,p)\|_{h,*}^2 &= \|(y,p)\|_h^2 + \varrho\,\theta \sum_{K\in\mathcal{T}_h} \|\lambda_h L_x y\|_{L_2(K)}^2 + 3\varrho\theta^{-1}\|\lambda_h^{-1} y\|_Q^2 \\ &\quad + \theta \sum_{K\in\mathcal{T}_h} \|\lambda_h L_x p\|_{L_2(K)}^2 + 3\theta^{-1}\|\lambda_h^{-1} p\|_Q^2. \end{aligned}$$

The boundedness constant μ_b will be defined below. At first, using integration by parts with respect to t, we get the identity

$$\begin{aligned} a_h(y,p;v_h,q_h) &= \int_Q p(v_h + \theta\lambda_h^2 \partial_t v_h)\,\mathrm{d}Q + \varrho \int_{\partial Q} y v_h n_t\,\mathrm{d}s - \varrho \int_Q y\,\partial_t v_h\,\mathrm{d}Q \\ &+ \varrho \int_Q (\theta\lambda_h^2 \partial_t y \partial_t v_h + \nu \nabla_x y \cdot \nabla_x v_h)\mathrm{d}Q + \varrho \sum_{K\in\mathcal{T}_h} \int_K \theta\lambda_h^2 L_x y\,\partial_t v_h\,\mathrm{d}K \\ &- \int_Q y(q_h - \theta\lambda_h^2 \partial_t q_h)\,\mathrm{d}Q - \int_{\partial Q} p q_h n_t\,\mathrm{d}s + \int_Q p\,\partial_t q_h\,\mathrm{d}Q \\ &+ \int_Q (\theta\lambda_h^2 \partial_t p \partial_t q_h + \nu \nabla_x p \cdot \nabla_x q_h)\mathrm{d}Q - \sum_{K\in\mathcal{T}_h} \int_K \theta\lambda_h^2 L_x p\,\partial_t q_h\,\mathrm{d}K \end{aligned}$$

that is valid for all $(y,p) \in (Y_{0h} + Y_0 \cap H^{L,1}(Q)) \times (P_{Th} + P_T \cap H^{L,1}(Q))$ and $(v_h, q_h) \in Y_{0h} \times P_{Th}$, and that is the starting point for estimating the right-hand side from above. Indeed, Young's and Cauchy's inequalities, and the generalized Friedrichs inequality (18), yield the following estimates:

$$\begin{aligned} a_h(y,p;v_h,q_h) &\le \varrho\|y(\cdot,T)\|_\Omega \|v_h(\cdot,T)\|_\Omega + \varrho\theta^{-1/2}\|\lambda_h^{-1} y\|_Q \theta^{1/2}\|\lambda_h \partial_t v_h\|_Q \\ &+ \varrho\theta\|\lambda_h \partial_t y\|_Q \|\lambda_h \partial_t v_h\|_Q + \varrho\|\sqrt{\nu}\nabla_x y\|_Q \|\sqrt{\nu}\nabla_x v_h\|_Q \\ &+ \Big(\sum_{K\in\mathcal{T}_h} \varrho\theta\|\lambda_h L_x y\|_K^2\Big)^{1/2} \Big(\sum_{K\in\mathcal{T}_h} \varrho\theta\|\lambda_h \partial_t v_h\|_K^2\Big)^{1/2} \\ &+ \theta^{-1/2}\|\lambda_h^{-1} p\|_Q \theta^{1/2}\|\lambda_h v_h\|_Q + \theta^{-1/2}\|\lambda_h^{-1} p\|_Q\, \theta^{3/2}\|\lambda_h^3 \partial_t v_h\|_Q \\ &+ \|p(\cdot,0)\|_\Omega \|q_h(\cdot,0)\|_\Omega + \theta^{-1/2}\|\lambda_h^{-1} p\|_Q \theta^{1/2}\|\lambda_h \partial_t q_h\|_Q \\ &+ \theta\|\lambda_h \partial_t p\|_Q \|\lambda_h \partial_t q_h\|_Q + \|\sqrt{\nu}\nabla_x p\|_Q \|\sqrt{\nu}\nabla_x q_h\|_Q \\ &+ \Big(\sum_{K\in\mathcal{T}_h} \theta\|\lambda_h L_x p\|_K^2\Big)^{1/2} \Big(\sum_{K\in\mathcal{T}_h} \theta\|\lambda_h \partial_t q_h\|_K^2\Big)^{1/2} \end{aligned}$$

$$
\begin{aligned}
&+\varrho^{1/2}\theta^{-1/2}\|\lambda_h^{-1}y\|_Q\,\varrho^{-1/2}\theta^{1/2}\|\lambda_h q_h\|_Q\\
&+\varrho^{1/2}\theta^{-1/2}\|\lambda_h^{-1}y\|_Q\,\varrho^{-1/2}\theta^{3/2}\|\lambda_h^3\partial_t q_h\|_Q\\
\le\ &\Big[\varrho\|y(\cdot,T)\|_\Omega^2+\varrho\theta^{-1}\|\lambda_h^{-1}y\|_Q^2+\varrho\theta\|\lambda_h\partial_t y\|_Q^2+\varrho\|\sqrt{\nu}\nabla_x y\|_Q^2\\
&+\varrho\sum_{K\in\mathcal{T}_h}\theta\|\lambda_h L_x y\|_K^2+\theta^{-1}\|\lambda_h^{-1}p\|_Q^2+\theta^{-1}\|\lambda_h^{-1}p\|_Q^2\\
&+\|p(\cdot,0)\|_\Omega^2+\theta^{-1}\|\lambda_h^{-1}p\|_Q^2+\theta\|\lambda_h\partial_t p\|_Q^2+\|\sqrt{\nu}\nabla_x p\|_Q^2\\
&+\sum_{K\in\mathcal{T}_h}\theta\|\lambda_h L_x p\|_K^2+\varrho\theta^{-1}\|\lambda_h^{-1}y\|_Q^2+\varrho\theta^{-1}\|\lambda_h^{-1}y\|_Q^2\Big]^{1/2}\\
&\times\Big[\varrho\|v_h(\cdot,T)\|_\Omega^2+\varrho\theta\|\lambda_h\partial_t v_h\|_Q^2+\varrho\theta\|\lambda_h\partial_t v_h\|_Q^2+\varrho\|\sqrt{\nu}\nabla_x v_h\|_Q^2\\
&+\varrho\theta\|\lambda_h\partial_t v_h\|_Q^2+\theta\|\lambda_h v_h\|_Q^2+\theta^2\overline{\lambda}_0^{-4}h^4\theta\|\lambda_h\partial_t v_h\|_Q^2\\
&+\|q_h(\cdot,0)\|_\Omega^2+\theta\|\lambda_h\partial_t q_h\|_Q^2+\theta\|\lambda_h\partial_t q_h\|_Q^2+\|\sqrt{\nu}\nabla_x q_h\|_Q^2\\
&+\theta\|\lambda_h\partial_t q_h\|_Q^2+\varrho^{-1}\theta\|\lambda_h q_h\|_Q^2+\varrho^{-1}\theta^2\overline{\lambda}_0^{-4}h^4\theta\|\lambda_h\partial_t q_h\|_Q^2\Big]^{1/2}\\
\le\ &\Big[\varrho\|y\|_{h,T}+\|p\|_{h,0}+\varrho\sum_{K\in\mathcal{T}_h}\theta\|\lambda_h L_x y\|_K^2+\sum_{K\in\mathcal{T}_h}\theta\|\lambda_h L_x p\|_K^2\\
&+(\varrho+\varrho+\varrho)\theta^{-1}\|\lambda_h^{-1}y\|_Q^2+(2+1)\theta^{-1}\|\lambda_h^{-1}p\|_Q^2\Big]^{1/2}\\
&\times\Big[\varrho\|v_h(\cdot,T)\|_\Omega^2+(3\varrho+\theta^2\overline{\lambda}_0^{-4}h^4)\theta\|\lambda_h\partial_t v_h\|_Q^2\\
&+(\varrho+\theta\overline{\lambda}_0^{-2}h^2c_F(\nu)^2)\|\sqrt{\nu}\nabla_x v_h\|_Q^2\\
&+\|q_h(\cdot,0)\|_\Omega^2+(3+\varrho^{-1}\theta^2\overline{\lambda}_0^{-4}h^4)\theta\|\lambda_h\partial_t q_h\|_Q^2\\
&+(1+\varrho^{-1}\theta\overline{\lambda}_0^{-2}h^2c_F(\nu)^2)\|\sqrt{\nu}\nabla_x q_h\|_Q^2\Big]^{1/2}\\
\le\ &\mu_b\|(y,p)\|_{h,*}\|(v_h,q_h)\|_h
\end{aligned}
$$

with $\mu_b = (\max\{3+\varrho^{-1}\theta^2\overline{\lambda}_0^{-4}h^4, 1+\theta\overline{\lambda}_0^{-2}h^2c_F(\nu)^2\varrho^{-1}\})^{1/2}$, where we use the shorter notations $\|\cdot\|_D$ for the L_2–norms $\|\cdot\|_{L_2(D)}$. The following best-approximation error estimate is now an easy consequence of the Galerkin orthogonality (15), the coercivity estimate (20), the extended boundedness estimate (22), and the triangle inequality.

Theorem 1. *Let us assume that the coefficient ν fulfills the conditions leading to maximal parabolic regularity, i.e. the unique solution (y,p) of the optimality system (8)–(9) belongs to the space $Y_0\cap H^{L,1}(Q)\times P_T\cap H^{L,1}(Q)$. Furthermore, let ϱ be some fixed positive regularization parameter, and let θ be a fixed scaling parameter such that condition (21) is satisfied. Then the discretization error estimate*

$$
\|(y,p)-(y_h,p_h)\|_h \le \inf_{(v_h,q_h)\in Y_{0h}\times P_{Th}}\big(\|(y,p)-(v_h,q_h)\|_h+\frac{\mu_b}{\mu_c}\|(y,p)-(v_h,q_h)\|_{h,*}\big) \tag{23}
$$

holds, where $(y_h,p_h)\in Y_{0h}\times P_{Th}$ is the unique solution of the finite element optimality system (14).

Under additional regularity assumptions imposed on the solution (y,p), the best-approximation error estimate (23) yields discretization error estimates in terms of the mesh-sizes. Indeed, choosing $v_h = I_h y \in Y_{0h}$ and $q_h = I_h p \in P_{Th}$ in the infimum at the right-hand side of (23), we can show the following theorem, where I_h is the usual nodal finite element interpolation operator for sufficiently smooth solutions $y, p \in H^{m+1}(Q) \subset C(\overline{Q})$ with $m+1 > (d+1)/2$, or a quasi-interpolation operator à la Clément [12] and Scott-Zhang [44] for low-regularity solutions $y, p \in H^{m+1}(Q)$ with $m > 0$; see also [8].

Theorem 2. *Let the assumptions of Theorem 1 hold. We further assume that all transformations $x_K(\cdot)$ from the reference element $\hat{K}$ to the physical finite element $K \in \mathcal{T}_h$ are affine-linear. Then, in the smooth case, when assuming $y, p \in \{v \in H^{m+1}(Q) : v|_K \in H^\ell(K)\, \forall K \in \mathcal{T}_h\}$ for some $\ell \geq m+1 > (d+1)/2$, we get the estimate*

$$\|(y,p)-(y_h,p_h)\|_h \leq \big(1+\frac{\mu_b}{\mu_c}\big)\left(\sum_{K\in\mathcal{T}_h} h_K^{2(s-1)}(c_1|y|^2_{H^s(K)} + c_2|p|^2_{H^s(K)})\right)^{1/2} \tag{24}$$

with $s = \min\{l, k+1\}$ and some generic positive constants c_1 and c_2, whereas, in the non-smooth case, when only assuming $y, p \in H^{m+1}(Q)$ for some $(d+1)/2 \geq m+1 > 1$, and $\nu\nabla_x u \in (H^m(K))^d$, we arrive at the estimate

$$\|(y,p)-(y_h,p_h)\|_h \leq \big(1+\frac{\mu_b}{\mu_c}\big)\left(\sum_{K\in\mathcal{T}_h} h_K^{2(s-1)}(c_3\mathcal{N}^2(y) + c_4\mathcal{N}^2(p))\right)^{1/2} \tag{25}$$

with $s = \min\{m+1, k+1\} = m+1 \leq (d+1)/2$ for $d = 2, 3$, and positive generic constants c_3 and c_4, where

$$\mathcal{N}^2(v) = |v|^2_{H^s(S_K)} + |\nu\nabla_x v|^2_{H^{s-1}(K)} + h_K^{4-2s}\|\mathrm{div}_x(\nu\nabla_x v)\|^2_{L_2(K)},$$

and $S_K := \{K' \in \mathcal{T}_h : \overline{K} \cap \overline{K}' \neq \emptyset\}$ denotes the neighborhood of the simplex $K \in \mathcal{T}_h$.

Proof. Using standard interpolation respectively quasi-interpolation error estimates (see, e.g., [12], [44], [8], and [21] for space interpolation in the case of semi-norms), we can derive the discretization error estimates (24) and (25) from the best-approximation error estimate (23) along the line of the proofs for the state equations given in [29] and [30] for the smooth and non-smooth cases, respectively. Indeed, in the norms of the right-hand side of (23), the same (quasi-) interpolation error terms appear as in the corresponding best-approximation error estimates in [29] and [30]. □

We mention that the semi-norms in the estimates (24) and (25) have to be replaced by the corresponding full norms in the case of non-affine linear mappings $x_K(\cdot)$ from $\hat{K}$ to $K \in \mathcal{T}_h$, e.g., if one uses the popular isoparametric elements ($k \geq 2$) or general non-linear mappings in order to represent (or approximate) curved interfaces or boundaries. Regularity results for the solution (y,p) of the optimality system (6)–(7) can be derived from known regularity results for parabolic initial-boundary value problems [16, 26, 27] by simple bootstrapping arguments. Here we always assume that the coefficient ν is as smooth as necessary.

In the case of low-regularity solutions when singularities in the time or/and space derivatives appear, the convergence rate is affected by these singularities, e.g., we observe $O(h^{s-1}) = O(h^m)$ instead of $O(h)$ for linear shape functions ($k = 1$) if (y, p) only belongs to $H^{1+m}(Q)$, where $s = \min\{1 + m, 2\} = 1 + m$ for $0 < m \leq 1$. The full rate $O(h)$ can be recovered by mesh grading that was already used for elliptic boundary value problems in early works by Oganesyan and Rukhovets [41]; see also [2] for more recent results. However, in order to use the mesh grading technique, we must know the strengths of the singularities and their positions in space and time. Thus, in practice, one wants to implement an adaptive finite element method (AFEM) that is based on local error indicators and automatic adaptive mesh refinement. Such an adaptive finite element code should do the same job as an a priori mesh grading.

7 Error indicators and adaptivity

In many practical applications, such low-regularity solutions can appear due to discontinuous coefficients, reentrant corners in the computational domain, changing boundary conditions, and missing compatibility of the boundary conditions with the initial conditions. Discontinuous target states y_d will lead to steep gradients, in particular, for small regularization parameters ϱ. We note that the target y_d can change discontinuously in space and time; cf. numerical example from Subsection 9.2. Hence, for such kind of non-smooth problems, it makes sense to use adaptive mesh refinements that are guided by local error indicators based on a posteriori error indicators or even estimators. The unstructured space-time approach considered in this paper allows for adaptivity in space and time simultaneously. This is a huge advantage of fully unstructured space-time techniques over the usual time-stepping methods or tensor-product techniques.

In order to drive the adaptive process, we will use the error indicator of residual type proposed by Steinbach and Yang in [47] for parabolic PDEs; see also [33] for applications to parabolic optimal control problems. In particular, given the finite element state y_h and co-state p_h, we compute the local indicator

$$\eta_K^2(y_h, p_h) = \eta_{K,y}^2(y_h, p_h) + \eta_{K,p}^2(y_h, p_h),$$

where

$$\begin{aligned}
\eta_{K,y}^2(y_h, p_h) &= h_K^2 \|\varrho(\partial_t y_h - \operatorname{div}_x(\nu \nabla_x y_h)) + p_h\|_K^2 + h_K \|\varrho[\![\nu \nabla_x y_h]\!]\|_{\partial K}^2 \text{ and} \\
\eta_{K,p}^2(y_h, p_h) &= h_K^2 \|y_h - y_d + \partial_t p_h + \operatorname{div}_x(\nu \nabla_x y_h)\|_K^2 + h_K \|[\![\nu \nabla_x p_h]\!]\|_{\partial K}^2
\end{aligned}$$

are nothing but the residual and jump terms of the coupled PDE optimality system in strong form (8)–(9), respectively. Once we have computed the indicators for each $K \in \mathcal{T}_h$, we determine a set $\mathcal{M}_h$ of (almost) minimal cardinality such that

$$\sigma \sum_{K \in \mathcal{T}_h} \eta_K^2(y_h, p_h) \leq \sum_{K \in \mathcal{M}_h} \eta_K^2(y_h, p_h)$$

where $\sigma \in (0, 1)$ is an a priori chosen bulk parameter. This marking strategy is called Dörfler marking [14]. The elements of the set $\mathcal{M}_h$ are then refined, where we might have to refine additional elements in order to maintain the conformity

and shape-regularity of the mesh; see, e.g., [35] and [49] for a bisection strategy for simplices that works in any dimension. We use this bisection strategy for our numerical experiments in Section 9 too.

8 Algebraic system and solvers

Let the finite element spaces $Y_{0h} = \mathrm{span}\{\phi_j : j = 1, \ldots, N_h\}$ and $P_{Th} = \{\psi_m : m = 1, \ldots, M_h\}$ be spanned by the standard nodal finite element basis. Then each finite element function $y_h \in Y_{0h}$ and $p_h \in P_{Th}$ can the represented in the form

$$y_h = \sum_{j=1}^{N_h} y_j \phi_j \quad \text{and} \quad p_h = \sum_{m=1}^{M_h} p_m \psi_m. \tag{26}$$

Inserting (26) into (14), and testing with basis functions $\phi^{(i)}$ and $\psi^{(n)}$, we obtain one big linear system

$$\mathbf{K}_h \begin{pmatrix} \mathbf{y}_h \\ \mathbf{p}_h \end{pmatrix} = \begin{pmatrix} \mathbf{0} \\ \mathbf{f}_h \end{pmatrix} \tag{27}$$

for determining the unknown coefficient vectors $\mathbf{y}_h = (y_j)_{j=1,\ldots,N_h} \in \mathbb{R}^{N_h}$ and $\mathbf{p}_h = (p_m)_{m=1,\ldots,M_h} \in \mathbb{R}^{M_h}$ at once for the whole space time cylinder, where $\mathbf{f}_h = (\ell_h(0, \psi_n))_{n=1,\ldots,M_h} \in \mathbb{R}^{M_h}$. The system matrix

$$\mathbf{K}_h = (a_h(\phi_j, \psi_m; \phi_i, \psi_n))_{i,j=1,\ldots,N_h}^{m,n=1,\ldots,M_h} = \begin{pmatrix} \mathbf{K}_{yy} & \mathbf{K}_{yp} \\ \mathbf{K}_{py} & \mathbf{K}_{pp} \end{pmatrix} \tag{28}$$

obviously has a 2×2 block structure with the blocks $\mathbf{K}_{yy}$, $\mathbf{K}_{yp}$, $\mathbf{K}_{py}$, and $\mathbf{K}_{pp}$ defined by the identities

$$\begin{aligned}
(\mathbf{K}_{yy}\mathbf{y}_h, \mathbf{v}_h) &= \varrho \int_Q \big(\partial_t y\, v + \theta\lambda_h^2 \partial_t y \partial_t v + \nu \nabla_x y \cdot \nabla_x v + \theta\lambda_h^2 L_x y\, \partial_t v\big) \mathrm{d}Q, \\
(\mathbf{K}_{yp}\mathbf{y}_h, \mathbf{q}_h) &= \int_Q y(q - \theta\lambda_h^2 \partial_t q) \mathrm{d}Q, \\
(\mathbf{K}_{py}\mathbf{p}_h, \mathbf{v}_h) &= \int_Q p(v + \theta\lambda_h^2 \partial_t v) \mathrm{d}Q, \\
(\mathbf{K}_{pp}\mathbf{p}_h, \mathbf{q}_h) &= \int_Q \big(-\partial_t p\, q + \theta\lambda_h^2 \partial_t p \partial_t q + \nu \nabla_x p \cdot \nabla_x q - \theta\lambda_h^2 L_x p\, \partial_t q\big) \mathrm{d}Q
\end{aligned}$$

for all coefficient vectors $\mathbf{y}_h, \mathbf{v}_h \in \mathbb{R}^{N_h}$ and $\mathbf{p}_h, \mathbf{q}_h \in \mathbb{R}^{M_h}$ corresponding to the finite element functions $y = y_h, v = v_h \in Y_{0h}$ and $p = p_h, q = q_h \in P_{Th}$ via the finite element isomorphism; cf. (26). Due to (20), the system matrix $\mathbf{K}_h$ as well as the diagonal blocks $\mathbf{K}_{yy}$ and $\mathbf{K}_{pp}$ are non-symmetric, but positive definite.

Hence the linear system (27) is solved by the FGMRES method [43], preconditioned by a block-diagonal AMG preconditioner $\mathbf{C}_h = \mathrm{blockdiag}(\mathbf{C}_{yy}, \mathbf{C}_{pp})$, where $\mathbf{C}_{yy} = \mathbf{K}_{yy}(\mathbf{I} - \mathbf{M}_{yy})^{-1}$ and $\mathbf{C}_{pp} = \mathbf{K}_{pp}(\mathbf{I} - \mathbf{M}_{pp})^{-1}$ with the AMG iteration matrices $\mathbf{M}_{yy}$ and $\mathbf{M}_{pp}$ resulting from one AMG V–cycles applied to the diagonal blocks of $\mathbf{K}_h$ using zero initial guesses [19]. In the next section, we test the performance of this AMG preconditioned FGMRES as single grid solver starting with initial guess zero and stopping after reducing the initial residual by the factor 10^{-8}, and in the nested iteration setting where the initial guess for

the refinement level $\ell + 1$ is interpolated from the last iterate at the preceding refinement level ℓ. The nested iteration approach aims at stopping the iteration when the corresponding discretization error is reached at level $\ell + 1$; see, e.g., [19].

9 Numerical Results

We implemented the space-time finite element scheme (14) using MFEM [38], a lightweight `C++` library. The block-diagonal AMG preconditioner described in Section 8 was realized by means of BoomerAMG, an AMG implementation provided by the linear solver library hypre[1]. Both libraries allow for easy parallelization. We stop the AMG preconditioned FGMRES iterations once the initial residual has been reduced by a factor of 10^{-8}. In the nested iteration approach, we stop the iteration when the residual computed from the interpolated coarse grid approximation is reduced by the factor 10^{-2} for linear elements, and by 10^{-3} for quadratic and cubic elements.

The adaptive bulk parameter is always chosen as $\sigma = 0.25$. In the following, we present the numerical results for two benchmark problems, which where already used in [33] and [31] as test problems, but for $d = 2$, i.e. $Q \subset \mathbb{R}^3$. Here we show the corresponding numerical results for the 4-dimensional space-time cylinder Q decomposed into shape-regular four-dimensional simplices (pentatopes).

9.1 Smooth problem with explicitly known solution

As first benchmark, we consider the space-time domain $Q = (0,1)^4$, i.e., $d = 3$, a constant diffusion coefficient $\nu \equiv 1$, and the manufactured state, co-state, and control

$$
\begin{aligned}
y(x,t) &= \sum_{i=1}^{d} \sin(x_i\,\pi)\left(a\,t^2 + b\,t\right),\\
p(x,t) &= -\varrho \sum_{i=1}^{d} \sin(x_i\,\pi)\left(d\,\pi^2\,a\,t^2 + (d\,\pi^2\,b + 2\,a)t + b\right) \text{ and}\\
u(x,t) &= \sum_{i=1}^{d} \sin(x_i\,\pi)\left(d\,\pi^2\,a\,t^2 + (d\,\pi^2\,b + 2\,a)t + b\right),
\end{aligned}
$$

respectively, where $a = -(2\pi^2 + 1)/(2\pi^2 + 2)$ and $b = 1$. The the desired state y_d is computed accordingly. This solution is highly smooth and has no local features. Hence, we expect to observe the optimal convergence rates predicted by Theorem 2. In Fig. 1, we present the convergence history of uniform refinements, for different polynomial degrees k, and a fixed regularization parameter $\varrho = 0.01$. Indeed, we always obtain a rate of $\mathcal{O}(h^k)$. Note that the "bumps" in the convergence rates are due to the bisection algorithm, where each uniform refinement only doubles the number of elements as opposed to the usual procedure of uniform refinements that subdivides each pentatope into 16 subpentatopes. Additionally, we also performed strong scaling tests for our AMG-preconditioned FGMRES solver; cf., Fig. 2. Here, we plot the solving

[1] https://computing.llnl.gov/projects/hypre-scalable-linear-solvers-multigrid-methods

time (including the setup time of the AMG preconditioner) for three different problem sizes, using linear elements for the left plot, and quadratic elements for the right plot. We can observe that, for linear elements, we obtain almost optimal scaling up to 64 cores, after which the speed up stagnates. This stagnation is due to fact that the problem sizes for each processor are too small, such that the parallel overhead is now the dominating factor. For quadratic elements, the overall speed up is optimal until 128 cores. Then the parallel overhead again affects the speed-up. We note that the size of the problems fitting to a single core can vary greatly depending on the polynomial degree k. Indeed, the biggest problem that we could solve on a single core has 2 084 994 dofs for linear elements, compared to 16 596 226 dofs for quadratic elements. Finally, we also

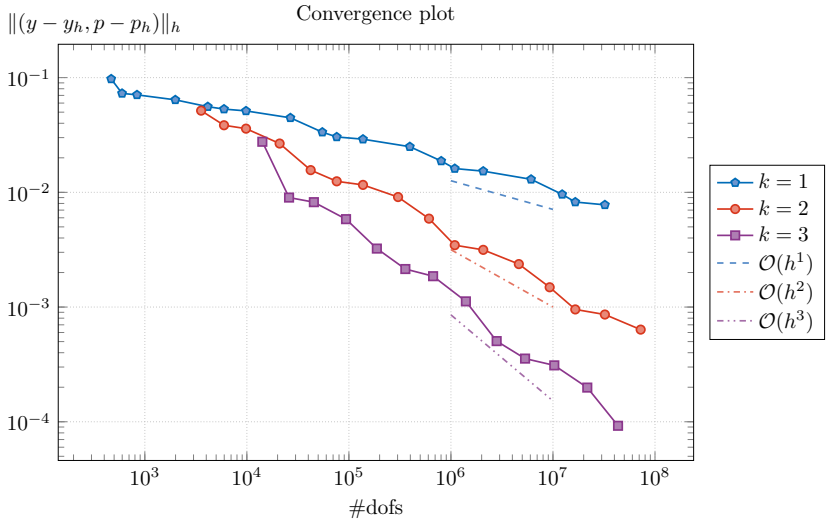

Fig. 1: Convergence rates in the mesh-dependent norm $\|(\cdot, \cdot)\|_h$ for different polynomial degrees k.

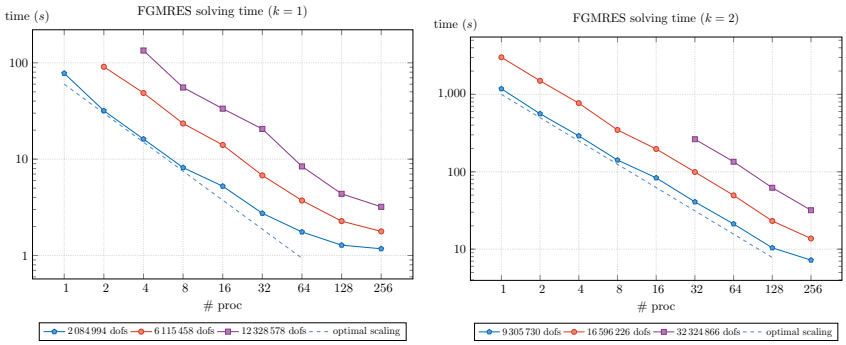

Fig. 2: Strong scaling results of the block-AMG preconditioned FGMRES for fixed problem sizes; using linear elements (left), and quadratic elements (right).

tested the linear solver in a nested iterations settings. In Tab. 1, we present the solving times and number of iterations, comparing non-nested and nested iter-

ations, for different polynomial degrees k. Here, we can deduce that the AMG preconditioner works very well in the nested iterations framework, reducing the number of iterations as well as the overall solving time drastically.

Tab. 1: Solving times and number of iterations for non-nested and nested iterations using 64 cores, where ℓ indicates the number of uniform refinements. The largest problem sizes are 32 278 018, 72 386 050, and 43 427 330 dofs, for the polynomial degrees $k = 1, 2$, and 3, respectively.

ℓ	$k=1$		$k=2$		$k=3$	
	non-nested	nested	non-nested	nested	non-nested	nested
0	11 (0.02 s)	13 (0.02 s)	21 (0.05 s)	26 (0.06 s)	44 (0.16 s)	55 (0.20 s)
4	13 (0.03 s)	3 (0.02 s)	28 (0.17 s)	10 (0.09 s)	47 (1.11 s)	17 (0.49 s)
8	16 (0.09 s)	4 (0.05 s)	37 (1.32 s)	14 (0.71 s)	62 (15.84 s)	20 (5.63 s)
12	21 (0.55 s)	4 (0.27 s)	49 (25.03 s)	13 (8.76 s)	83 (390.99 s)	20 (111.00 s)
15	30 (4.57 s)	4 (1.56 s)	70 (380.27 s)	10 (76.67 s)	–	–
16	28 (10.39 s)	4 (3.94 s)	–	–	–	–
18	40 (55.35 s)	2 (11.35 s)	–	–	–	–

9.2 Discontinuous target function

In order to showcase the adaptive capabilities of a space-time scheme, we once more consider the four-dimensional space-time domain, $Q = (0, 1)^4$, and a constant diffusion coefficient $\nu \equiv 1$. However, we now want to approximate the discontinuous desired state

$$y_d(x,t) = \begin{cases} 1 & \sqrt{|x-0.5|^2 + (t-0.5)^2} \leq \dfrac{1}{4} \\ 0 & \text{otherwise,} \end{cases}$$

that is nothing but a first expanding and then contracting ball, which is however fixed in space-time. Moreover, we use a smaller, fixed regularization parameter $\rho = 10^{-6}$. The discontinuity at the interface between the ball and its surrounding introduces steep gradients for the state and co-state, which require a rather fine local mesh-size in order to resolve the rapid changes properly. Hence, this problem is well suited for using adaptive refinements, driven by the error indicator introduced in Section 7. Indeed, the residual indicator leads to mesh refinements concentrated along the hypersurface of discontinuity; see Fig. 4, where we plot the finite element state y_h, co-state p_h, and control u_h on cuts through the space-time mesh $\mathcal{T}_h$. These cuts are nothing but unit cubes, which we then further cut by three planes along the three spatial coordinates centered at $(0.5, 0.5, 0.5)$. While we do not have explicit knowledge about the exact solutions, we can take a look at the convergence behavior of the sum of local indicators $\eta(y_h, p_h)^2 = \sum_{K\in\mathcal{T}_h} \eta_K(y_h, p_h)^2$; cf. Fig. 3. Here we can indeed observe almost optimal rates of $\mathcal{O}(h^k)$ in terms of $h = \text{dofs}^{-1/(d+1)}$. However, in contrast to residual estimators for elliptic problems, where the sum of indicators is indeed proportional to the discretization error in the energy norm (see, e.g., [9]), no such result is available for residual indicators for parabolic problems on totally unstructured space-time decompositions.

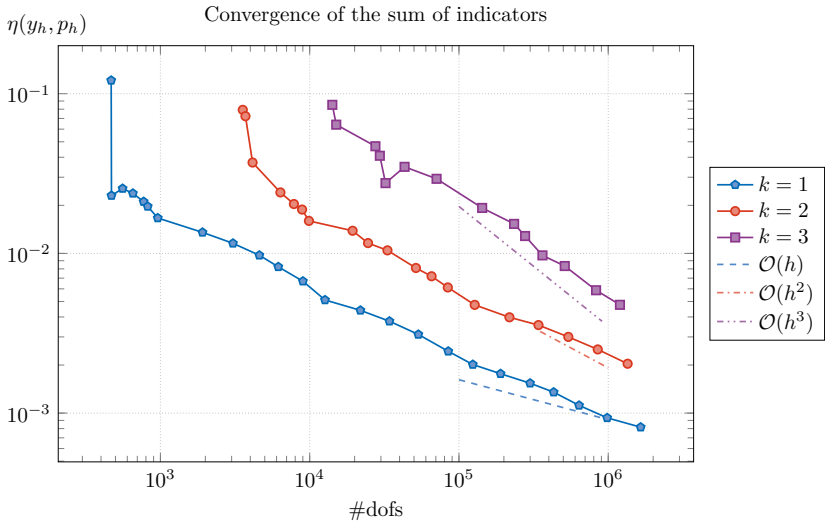

Fig. 3: Convergence plot of the sum of local error indicators $\eta^2(y_h, p_h) = \sum_{K \in \mathcal{T}_h} \eta_K^2(y_h, p_h)$ for different polynomial degrees k.

10 Conclusions and outlook

We presented and analyzed new locally stabilized space-time finite element schemes on fully unstructured, but shape regular simplicial decompositions of the space-time cylinder Q for the numerical solution of parabolic optimal control problems. Such meshes typically arise from adaptive mesh refinement driven by local error indicators. The meshes are described by a continuous, elementwise differentiable mesh density function $\lambda_h(x,t)$ that also provides the right scaling of the time-upwind test functions. The resulting space-time finite element scheme is consistent, coercive, and bounded. The boundedness of the corresponding bilinear form $a_h(\cdot;\cdot)$ holds for an extended space with respect to the first couple of functions. Beside the finite element functions, this space also contains the solution $(y,p) \in (Y_0 \cap H^{L,1}(Q)) \times (P_T \cap H^{L,1}(Q))$ in the maximal parabolic regularity setting. Coercivity, extended boundedness, and Galerkin orthogonality, which results from consistency, immediately yield a best-approximation estimate from which convergence rate estimates follow under additional regularity assumptions. The adaptive version of our space-time finite element method is based on residual error indicators, which work well in our numerical experiment. However, there is no theory concerning reliability, efficiency, convergence, and optimality in sense of the paper [9]. Finally, we have to solve one big system of finite element equations providing the finite element solution of the reduced optimality system all at once. We used a parallel version of an AMG preconditioned FGMRES that shows a excellent parallel performance in our numerical experiments. The construction and analysis of parallel solvers that are not only robust with respect to h and k, but also with respect to small regularization parameters ϱ is certainly a challenging task for future work. Simultaneous adaptivity and parallelization in space and time are big advantages of our really unstructured space-time finite element solver for the reduced optimality system that is forward and backward in time anyway. It

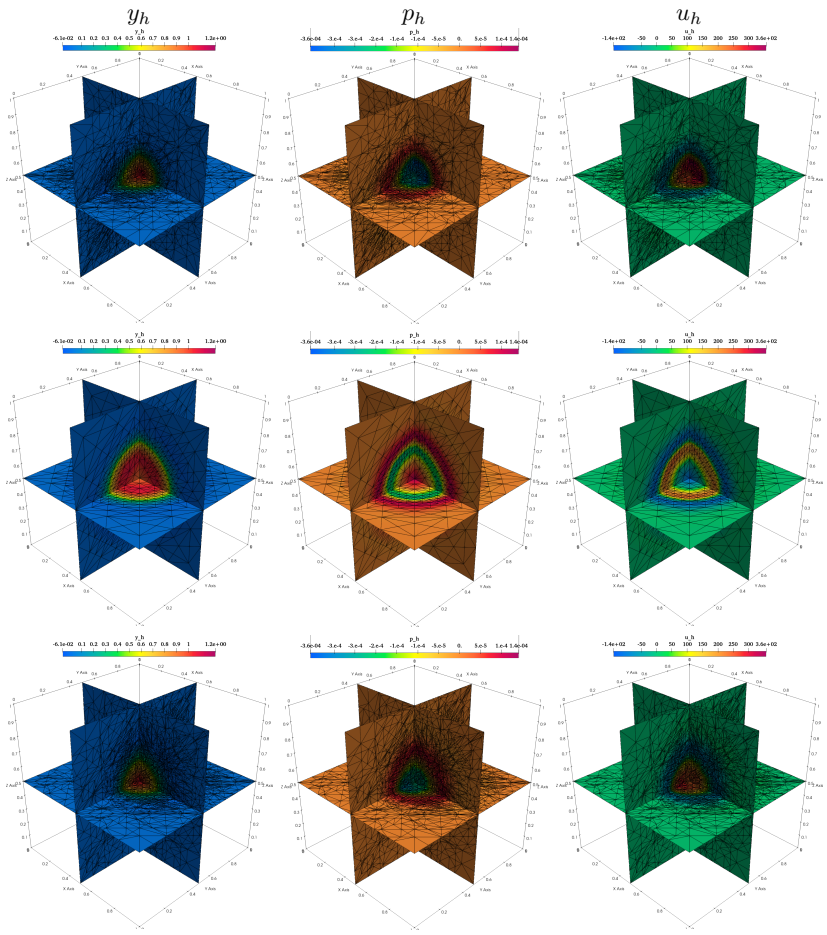

Fig. 4: Plots of the finite element functions y_h, p_h, and u_h over the mesh, cut at $t = 0.3$ (upper row); at $t = 0.5$ (middle row); and at $t = 0.7$ (bottom row).

is clear that this space-time technique can be applied to other optimal control problems and to other state equations including convection-diffusion problems and PDE system like the Navier-Stokes equations.

References

[1] Adams, R., and Fournier, J. *Sobolev Spaces.* Academic Press & Elsevier, 2003.

[2] Apel, T., Sändig, A.-M., and Whiteman, J. R. Graded mesh refinement and error estimates for finite element solutions of elliptic boundary value problems in non-smooth domains. *Math. Methods Appl. Sci. 19*, 30 (1996), 63–85.

[3] Babuška, I. Error-bounds for finite element method. *Numer. Math. 16*, 4 (1971), 322–333.

[4] Babuška, I., and Aziz, A. Survey lectures on the mathematical foundation of the finite element method. In *The Mathematical Foundations of the Finite Element Method with Applications to Partial Differential Equations* (New York, 1972), Academic Press, pp. 1–359.

[5] Bank, R., Vassilevski, P., and Zikatanov, L. Arbitrary dimension convection-diffusion schemes for space-time discretizations. *J. Comput. Appl. Math. 310* (2017), 19–31.

[6] Borzì, A., and Schulz, V. *Computational optimization of systems governed by partial differential equations*, vol. 8 of *Computational Science & Engineering*. Society for Industrial and Applied Mathematics (SIAM), 2011.

[7] Braess, D. *Finite Elements. Theory, Fast Solvers and Applications in Solid Mechanics*. Cambridge University Press, 2007.

[8] Brenner, S. C., and Scott, L. R. *The mathematical theory of finite element methods*, third ed., vol. 15 of *Texts in Applied Mathematics*. Springer, New York, 2008.

[9] Carstensen, C., Feischl, M., Page, M., and Praetorius, C. Axioms of adaptivity. *Comput. Methods Appl. Math. 67* (2014), 1195–1253.

[10] Casas, E., Clason, C., and Kunisch, K. Parabolic control problems in measure spaces with sparse solutions. *SIAM J. Control Optim. 51*, 1 (2013).

[11] Casas, E., Mateos, M., and Rösch, A. Improved approximation rates for a parabolic control problem with an objective promoting directional sparsity. *Comput. Optim. Appl. 70* (2018), 239–266.

[12] Clément, P. Approximation by finite element functions using local regularization. *Rev. Française Automat. Informat. Recherche Opérationnelle Sér. 9*, R-2 (1975), 77–84.

[13] Dier, D. Non-autonomous maximal regularity for forms of bounded variation. *J. Math. Anal. Appl. 425* (2015), 33–54.

[14] Dörfler, W. A convergent adaptive algorithm for Poisson's equation. *SIAM J. Numer. Anal. 33*, 3 (1996), 1106–1124.

[15] Ern, A., and Guermond, J.-L. *Theory and Practice of Finite Elements*. Springer, NY, 2004.

[16] Evans, L. *Partial Differential Equations*, vol. 19 of *Graduate Studies in Mathematics*. American Mathematical Society, 2010.

[17] Fackle, S. J.-L. Lions' problem concerning maximal regularity of equations governed by non-autonomous forms. *Ann. I. H. Poincaré 34* (2017), 699–709.

[18] Gong, W., Hinze, M., and Zhou, Z. Space-time finite element approximation of parabolic optimal control problems. *J. Numer. Math. 20*, 2 (2012), 111–145.

[19] Haase, G., and Langer, U. Multigrid methods: From geometrical to algebraic versions. In *Modern Methods in Scientific Computing and Applications*, A. Bourlioux, M. Gander, and G. Sabidussi, Eds. Kluwer Academic Press, Dordrecht, 2002, pp. 103–154.

[20] Herzog, R., Stadler, G., and Wachsmuth, G. Directional sparsity in optimal control of partial differential equations. *SIAM J. Control Optim. 50*, 2 (2012), 943–963.

[21] Heuer, N. On the equivalence of fractional-order Sobolev semi-norms. *J. Math. Anal. Appl. 417*, 2 (2014), 505–518.

[22] Hinze, M., Pinnau, R., Ulbrich, M., and Ulbrich, S. *Optimization with PDE Constraints*, vol. 23. Springer-Verlag, Berlin, 2009.

[23] Hughes, T., and Brooks, A. A multidimensional upwind scheme with no crosswind diffusion. In *Finite Element Methods for Convection Dominated Flows* (New York, 1979), T. Hughes, Ed., vol. 34 of *AMD*, ASME.

[24] Hughes, T., Franca, L., and Hulbert, G. A new finite element formulation for computational fluid dynamics: VIII. The Galerkin/least-squares method for advection-diffusive equations. *Comput. Methods Appl. Mech. Engrg. 73* (1989), 173–189.

[25] Johnson, C., and Saranen, J. Streamline diffusion methods for the incompressible Euler and Navier-Stokes equations. *Math. Comp. 47*, 175 (1986), 1–18.

[26] Ladyžhenskaya, O. A. *The boundary value problems of mathematical physics*, vol. 49 of *Applied Mathematical Sciences*. Springer-Verlag, New York, 1985. Translated from the Russian edition, Nauka, Moscow, 1973.

[27] Ladyzhenskaya, O. A., Solonnikov, V. A., and Uraltseva, N. *Linear and quasilinear equations of parabolic type*. Nauka, Moscow, 1967.

[28] Langer, U., Moore, S., and Neumüller, M. Space-time isogeometric analysis of parabolic evolution equations. *Comput. Methods Appl. Mech. Engrg. 306* (2016), 342–363.

[29] Langer, U., Neumüller, M., and Schafelner, A. Space-time finite element methods for parabolic evolution problems with variable coefficients. In *Advanced Finite Element Methods with Applications - Selected Papers from the 30th Chemnitz Finite Element Symposium 2017*, T. Apel, U. Langer, A. Meyer, and O. Steinbach, Eds., vol. 128 of *LNCSE*. Springer, Berlin, Heidelberg, New York, 2019, ch. 13, pp. 229–256.

[30] Langer, U., and Schafelner, A. Adaptive space-time finite element methods for non-autonomous parabolic problems with distributional sources. *Computational Methods in Applied Mathematics 20*, 4 (2020), 677–693.

[31] Langer, U., and Schafelner, A. Simultaneous space-time finite element methods for parabolic optimal control problems. Tech. Rep. arXiv:2103.01688 [math.NA], arXiv, 2021.

[32] Langer, U., Steinbach, O., Tröltzsch, F., and Yang, H. Space-time finite element discretization of parabolic optimal control problems with energy regularization. *SIAM Journal on Numerical Analysis 59*, 2 (2021), 660–674.

[33] Langer, U., Steinbach, O., Tröltzsch, F., and Yang, H. Unstructured space-time finite element methods for optimal control of parabolic equation. *SIAM Journal on Scientific Computing 43*, 2 (2021), A744–A771.

[34] Lions, J. L. *Contrôle optimal de systèmes gouvernés par des équations aux dérivées partielles*. Dunod Gauthier-Villars, Paris, 1968.

[35] Maubach, J. M. Local bisection refinement for n-simplicial grids generated by reflection. *SIAM J. Sci. Comput. 16*, 1 (1995), 210–227.

[36] Meidner, D., and Vexler, B. A priori error estimates for space-time finite element discretization of parabolic optimal control problems. Part I: Problems without control constraints. *SIAM J. Control Optim. 47*, 3 (2008), 1150–1177.

[37] Meidner, D., and Vexler, B. A priori error estimates for space-time finite element discretization of parabolic optimal control problems. Part II: Problems with control constraints. *SIAM J. Control Optim. 47*, 3 (2008), 1301–1329.

[38] MFEM: Modular finite element methods library. mfem.org.

[39] Neitzel, I., Prüfert, U., and Slawig, T. A smooth regularization of the projection formula for constrained parabolic optimal control problems. *Numer. Funct. Anal. Optim. 33*, 12 (2011), 1283–1315.

[40] Nečas, J. Sur une méthode pour résoudre les équations aux dérivées partielles du type elliptique, voisine de la variationnelle. *Ann. Scuola Norm. Sup. Pisa 16*, 4 (1962), 305–326.

[41] Oganesjan, L., and Ruchovetz, L. *Variational Difference Methods for the Solution of Elliptic Equations*. Isdatelstvo Akademi Nank Armjanskoj SSR, Erevan, 1979. (in Russian).

[42] Repin, S. *A posteriori estimates for partial differential equations*, vol. 4 of *RSCAM*. de Gruyter, Berlin, 2008.

[43] Saad, Y. *Iterative Methods for Sparse Linear Systems*, second ed. Society for Industrial and Applied Mathematics (SIAM), Philadelphia, 2003.

[44] Scott, L. R., and Zhang, S. Finite element interpolation of nonsmooth functions satisfying boundary conditions. *Math. Comput. 54*, 190 (1990), 483–493.

[45] Stadler, G. Elliptic optimal control problems with L^1-control cost and applications for the placement of control devices. *Comput. Optim. Appl. 44* (2009), 159–181.

[46] Steinbach, O. Space-time finite element methods for parabolic problems. *Comput. Methods Appl. Math. 15*, 4 (2015), 551–566.

[47] Steinbach, O., and Yang, H. Comparison of algebraic multigrid methods for an adaptive space-time finite-element discretization of the heat equation in 3d and 4d. *Numer. Linear Algebra Appl. 25*, 3 (2018), e2143 nla.2143.

[48] Steinbach, O., and Yang, H. Space-time finite element methods for parabolic evolution equations: discretization, a posteriori error estimation, adaptivity and solution. In *Space-Time Methods: Application to Partial Differential Equations* (Berlin, 2019), O. Steinbach and U. Langer, Eds., vol. 25 of *RSCAM*, de Gruyter, pp. 207–248.

[49] Stevenson, R. The completion of locally refined simplicial partitionscreated by bisection. *Math. Comp. 77*, 261 (2008), 227–241.

[50] Tröltzsch, F. *Optimal control of partial differential equations: Theory, methods and applications*, vol. 112 of *Graduate Studies in Mathematics*. American Mathematical Society, Providence, Rhode Island, 2010.

Technical Reports of the Doctoral Program "Computational Mathematics"

2021

2021-01 J. Qi: *A tree-based algorithm on monomials in the Chow group of zero cycles in the moduli space of stable pointed curves of genus zero* Jan 2021. Eds.: S. Radu, J. Schicho

2021-02 A. Jiménez Pastor, P. Nuspl, V. Pillwein: *On C^2-finite sequences* Feb 2021. Eds.: M. Kauers, P. Paule

2021-03 A. Jiménez Pastor: *Simple differentially definable functions* Feb 2021. Eds.: M. Kauers, V. Pillwein

2021-04 U. Langer, A. Schafelner: *Simultaneous space-time finite element methods for parabolic optimal control problems* March 2021. Eds.: V. Pillwein, R. Ramlau

2021-05 U. Langer, A. Schafelner: *Space-time hexahedral finite element methods for parabolic evolution problems* March 2021. Eds.: B. Jüttler, V. Pillwein

2021-06 D. Jodlbauer, U. Langer, T. Wick: *Efficient monolithic solvers for fluid-structure interaction applied to flapping membranes* April 2021. Eds.: B. Jüttler, V. Pillwein

2021-07 U. Langer, A. Schafelner: *Adaptive space-time finite element methods for parabolic optimal control problems* May 2021. Eds.: V. Pillwein, R. Ramlau

2020

2020-01 N. Smoot: *A Single-Variable Proof of the Omega SPT Congruence Family Over Powers of 5* Feb 2020. Eds.: P. Paule, S. Radu

2020-02 A. Schafelner, P.S. Vassilevski: *Numerical Results for Adaptive (Negative Norm) Constrained First Order System Least Squares Formulations* March 2020. Eds.: U. Langer, V. Pillwein

2020-03 U. Langer, A. Schafelner: *Adaptive space-time finite element methods for non-autonomous parabolic problems with distributional sources* March 2020. Eds.: B. Jüttler, V. Pillwein

2020-04 A. Giust, B. Jüttler, A. Mantzaflaris: *Local (T)HB-spline projectors via restricted hierarchical spline fitting* March 2020. Eds.: U. Langer, V. Pillwein

2020-05 K. Banerjee, M. Ghosh Dastidar: *Hook Type Tableaux and Partition Identities* June 2020. Eds.: P. Paule, S. Radu

2020-06 A. Bostan, F. Chyzak, A. Jiménez-Pastor, P. Lairez: *The Sage Package* `comb_walks` *for Walks in the Quarter Plane* June 2020. Eds.: M. Kauers, V. Pillwein

2020-07 A. Meddah: *A stochastic multiscale mathematical model for low grade Glioma spread* June 2020. Eds.: E. Buckwar, V. Pillwein

2020-08 M. Ouafoudi: *A Mathematical Description for Taste Perception Using Stochastic Leaky Integrate-and-Fire Model* June 2020. Eds.: E. Buckwar, V. Pillwein

2020-09 A. Bostan, A. Jiménez-Pastor: *On the exponential generating function of labelled trees* July 2020. Eds.: M. Kauers, V. Pillwein

2020-10 J, Forcan, J. Qi: *How fast can Dominator win in the Maker-Breaker domination game?* July 2020. Eds.: V. Pillwein, J. Schicho

2020-11 J. Qi: *A calculus for monomials in Chow group of zero cycles in the moduli space of stable curves* Sept 2020. Eds.: P. Paule, J. Schicho

2020-12 J. Qi, J. Schicho: *Five Equivalent Ways to Describe a Phylogenetic Tree* November 2020. Eds.: M. Kauers, S. Radu

The complete list since 2009 can be found at
`https://www.dk-compmath.jku.at/publications/`

Doctoral Program
"Computational Mathematics"

Director:

Assoc. Prof. Dr. Veronika Pillwein
Research Institute for Symbolic Computation

Deputy Director:

Prof. Dr. Bert Jüttler
Institute of Applied Geometry

Address:

Johannes Kepler University Linz
Doctoral Program "Computational Mathematics"
Altenbergerstr. 69
A-4040 Linz
Austria
Tel.: ++43 732-2468-6840

E-Mail:

office@dk-compmath.jku.at

Homepage:

http://www.dk-compmath.jku.at

Submissions to the DK-Report Series are sent to two members of the Editorial Board who communicate their decision to the Managing Editor.